

Different dependence of narrow H α line luminosity on optical continuum luminosity between starforming galaxies and Type-2 AGN: globally negative AGN feedback in local Type-2 AGN?

XUEGUANG ZHANG^{*1}

¹Guangxi Key Laboratory for Relativistic Astrophysics, School of Physical Science and Technology, Guangxi University, Nanning, 530004, P. R. China

Submitted to ApJ

ABSTRACT

In this manuscript, clues are provided to support globally negative AGN feedback on star formation in the host galaxies of the local low-redshift SDSS Type-2 AGN, based on the different dependence of narrow H α line luminosity $L_{H\alpha}$ on optical continuum luminosity λL_{cont} between the starforming galaxies and the Type-2 AGN. Through the measured $L_{H\alpha}$ and λL_{cont} in SDSS starforming galaxies, there is a strong linear correlation between λL_{cont} and $L_{H\alpha}$, accepted as a standard correlation without effects of AGN activity. Meanwhile, considering apparent contributions of AGN activity to narrow H α line emissions in the Type-2 AGN, the correlation between λL_{cont} and $L_{H\alpha}$ in the SDSS Type-2 AGN leads to statistically lower $L_{H\alpha}$ in the Type-2 AGN than in the starforming galaxies, with significance level higher than 5σ , even after considering necessary effects (including effects of host galaxy properties), leading to accepted conclusion on the globally negative AGN feedback in the local Type-2 AGN. Meanwhile, properties of Dn(4000) and H δ_A can provide indirect clues to support the globally negative AGN feedback in the local Type-2 AGN, due to older stellar ages in the Type-2 AGN. Moreover, it is interesting to expect more than 50% narrow H α emissions globally suppressed in the host galaxies of the Type-2 AGN relative to the starforming galaxies. The results not only support globally negative AGN feedback in the local Type-2 AGN, but also show further clues on the quantification of suppressions of star formation by the globally negative AGN feedback.

Keywords: galaxies:active - galaxies:nuclei - quasars:emission lines - galaxies:Seyfert

1. INTRODUCTION

AGN feedback through galactic-scale outflows plays a key role in galaxy evolution, leading to the tight connections between Active Galactic Nuclei (AGN) and host galaxies (McNamara & Nulsen 2007; Fabian 2012; Gaspari et al. 2012; Kormendy & Ho 2012; Heckman & Best 2014; King & Pounds 2015; Tombesi et al. 2015; Muller-Sanchez et al. 2018; Baron et al. 2018; Russell et al. 2019; Kolokythas et al. 2020; Richard-Laferrriere et al. 2020; Chadayammuri et al. 2021; Kawamuro et al. 2021; Smethurst et al. 2021; Piotrowska et al. 2022). Both observational and theoretical results have shown clear impacts of either positive or negative AGN feedback on star formation in the host galaxies of AGN. Feruglio et al. (2010) have reported observational evidence to support negative AGN feedback in the nearest quasar Mrk 231, due to the detected giant molecular outflow with higher mass rate than the detected star formation rate in the host galaxy, therefore halting star formation. Page et al. (2012) have shown evidence to support negative AGN feedback, because rapid star formations are common in AGN host galaxies but that the most vigorous star formations cannot be observed in AGN with X-ray luminosities larger than $10^{44}\text{erg} \cdot \text{s}^{-1}$. Wylezalek & Zakamska (2016) have reported evidence for the negative AGN feedback, based on the AGN with strong outflow signatures being hosted in galaxies that are more quenched than galaxies with weaker outflow signatures. Comerford et al. (2020) have also shown evidence to support the negative AGN feedback, based on inside-out quenching of star formations in radio-mode AGN host galaxies which have older stellar populations through a sample of 406 AGN subdivided into radio-quiet and radio-mode AGN. Meanwhile, evidence to support positive AGN feedback can be found in the literature. Zubovas et al. (2013) have discussed the positive

AGN feedback in gas-rich phases by over-compressing cold dense gas. Zinn et al. (2013) have shown the positive AGN feedback, because much higher star formation rates in the AGN with pronounced radio jets than in the purely X-ray-selected ones. Shin et al. (2019) have reported positive feedback scenario in NGC 5728, due to higher star formation rates in the encountering region where the ionized gas outflows encounter the star formation ring at 1kpc radius. Mahoro et al. (2022) have shown that there are no apparent signs of negative AGN feedback, after comparing host galaxy properties of far-infrared AGN and non-AGN green valley galaxies. Therefore, it is interesting to provide further clues on the contradictory effects of AGN feedback on star formations, through different methods, which is the main objective of this manuscript.

Optical spectroscopic properties of starforming galaxies with no contribution of central AGN activity can be well applied to trace starforming histories, leading to the strong dependence of the star formation rates (SFRs) on the narrow $H\alpha$ line luminosities ($L_{H\alpha}$) in galaxies as well discussed in Sanchez (2020); Madau & Dickinson (2014); Kennicutt & Evans (2012); Kennicutt et al. (1994); Pflamm-Altenburg et al. (2007); Smit et al. (2016); Ly et al. (2011); Villa-Velez et al. (2021):

$$SFRs \propto L_{H\alpha}^{\beta} \quad (1)$$

. In this manuscript, among all the narrow emission-line main galaxies in SDSS DR16 (Sloan Digital Sky Survey, Data Release 16) (Ahumada et al. 2020), starforming galaxies with high-quality narrow emission lines can be collected, based on the dividing line applied in the BPT diagram (Baldwin et al. 1981; Kauffmann et al. 2003a; Kewley et al. 2006, 2013, 2019; Kauffmann et al. 2003; Zhang et al. 2020; Zhang 2022a) through the narrow emission line flux ratios of $[O\ III]\lambda 5007\text{\AA}$ to $H\beta$ (O3HB) and of $[N\ II]\lambda 6583\text{\AA}$ to $H\alpha$ (N2HA), which will be discussed in Section 2. Based on properties of continuum emissions and narrow $H\alpha$ emissions of the starforming galaxies with no contribution of AGN activity on the spectroscopic features, dependence of narrow $H\alpha$ line luminosity on optical continuum luminosity λL_{cont} in the starforming galaxies can be used as a standard candle to check effects of AGN feedback in Type-2 AGN.

Not similar as the starforming galaxies, Type-2 AGN have optical spectroscopic narrow emission lines including apparent contributions of central AGN activity. Based on commonly accepted and constantly being improved unified model (Netzer 2015; Suh et al. 2019) of AGN, emissions from central accretion disks and from central broad emission line regions are totally obscured by central dust torus (Davies et al. 2015; Netzer et al. 2016; Martinez-Paredes et al. 2017; Zhuang et al. 2018; Prieto et al. 2021; Zhang 2022b, 2023) in the Type-2 AGN. Therefore, narrow emission lines of Type-2 AGN have contributions from both central AGN activity and starforming, however, both the continuum emissions and the narrow absorption features in host galaxies of the Type-2 AGN have few contributions of central AGN activity, which are strongly supported by optical spectra (with emission line features being masked out) of Type-2 AGN described by pure stellar templates without considerations of AGN contributions as discussed in Section 3. Hence, studying properties of the narrow $H\alpha$ emissions in a large sample of Type-2 AGN can provide clues on effects of AGN feedback, after considering effects of AGN activity on the observational narrow $H\alpha$ line emissions but few effects on the observational continuum emissions in the host galaxies of Type-2 AGN.

The manuscript is organized as follows. Section 2 presents the data samples of starforming galaxies and Type-2 AGN. Section 3 presents our main results and necessary discussions. Section 4 gives our summary and conclusions. And in this manuscript, we have adopted the cosmological parameters of $H_0 = 70\text{km} \cdot \text{s}^{-1}\text{Mpc}^{-1}$, $\Omega_{\Lambda} = 0.7$ and $\Omega_m = 0.3$.

2. DATA SAMPLES

All the low redshift ($z < 0.35$) main galaxies with high-quality spectra (median spectral signal-to-noise ratio S/N larger than 20) are firstly collected from SDSS DR16, through the SDSS provided SQL (Structured Query Language) Search tool (<http://skyserver.sdss.org/dr16/en/tools/search/sql.aspx>) by the following query

```
SELECT S.plate , S.fiberid , S.mjd , S.z , S.snmedian ,
       P.petroR50_u , P.petroR50err_u , P.petroR50_g , P.petroR50err_g ,
       P.petroR50_r , P.petroR50err_r , P.petroR50_i , P.petroR50err_i ,
       P.petroR50_z , P.petroR50err_z , P.petroR90_u , P.petroR90err_u ,
       P.petroR90_g , P.petroR90err_g , P.petroR90_r , P.petroR90err_r ,
       P.petroR90_i , P.petroR90err_i , P.petroR90_z , P.petroR90err_z ,
       P.devab_u , P.devab_g , P.devab_r , P.devab_i , P.devab_z ,
       M.mstellar_median , M.mstellar_err
FROM SpecObjall as S JOIN PhotoObjAll as P ON S.bestobjid = P.objid
JOIN stellarMassPCAWiscM11 as M ON M.specobjid = S.specobjid
WHERE S.class='GALAXY' and S.z<0.35 and S.zwarning=0 and S.snmedian > 20
```

Here, the restriction $z < 0.35$ is applied, to ensure that the narrow $H\alpha$ and the $[N\ II]$ emission lines to be totally covered in the SDSS spectra, which will be used to do classifications of the main galaxies through the BPT diagrams. Meanwhile, properties

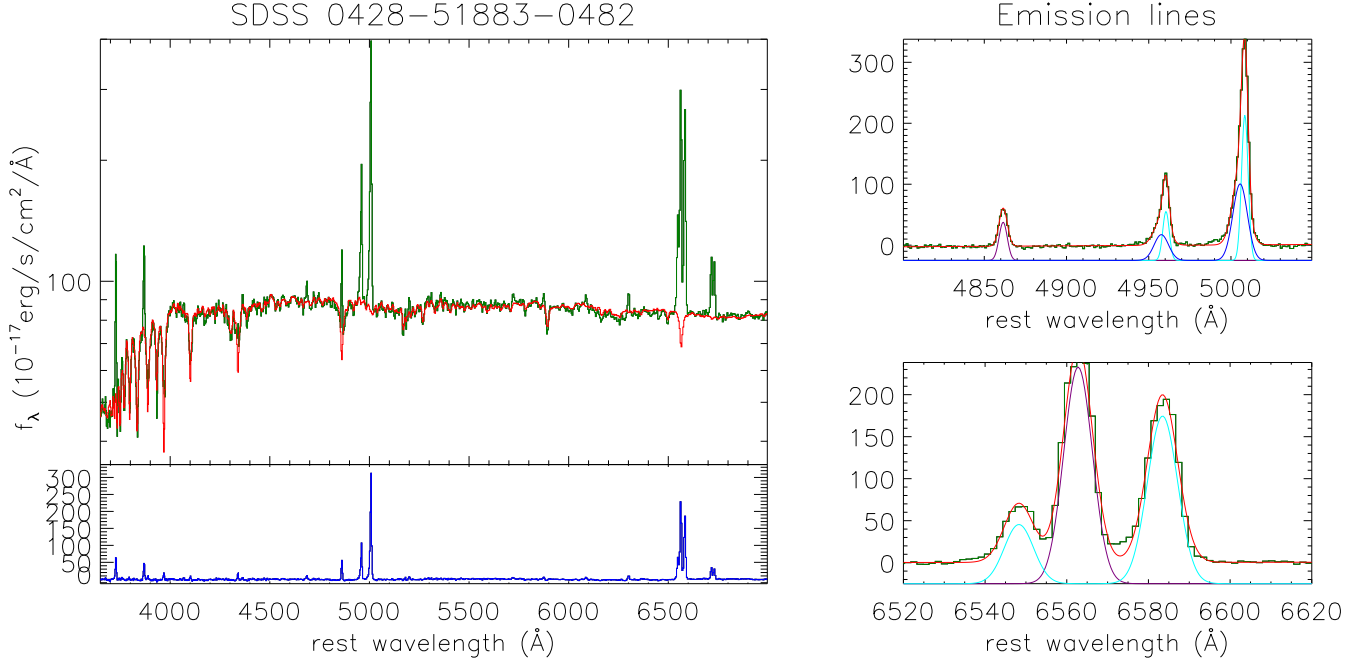


Figure 1. Left panels show examples on the SSP method determined stellar continuum (in top left panel) and the corresponding line spectrum (in bottom left panel) in the Type-2 AGN SDSS 0533-51994-0031. Right panels show the corresponding best fitting results to the emission lines, after subtractions of the determined stellar continuum. In the left panels, solid lines in dark green, red and blue represent the observed SDSS spectrum, the SSP method determined stellar continuum and the line spectrum after subtractions of the stellar continuum, respectively. In right panels, solid dark green line shows the line spectrum, solid red line shows the best-fitting results. In the top right panel, solid purple line shows the determined narrow H β , solid cyan lines and solid blue lines show the determined core and shifted-wing related broad components of [O III] doublet, respectively. In the bottom right panel, solid purple line and solid cyan lines show the determined narrow H α and [N II] doublet, respectively. In the top left panel, in order to show clearer absorption features, the Y-axis is shown in logarithmic coordinate.

of the inverse concentration parameter IC will be discussed in Section 3, therefore, the SDSS public database of 'PhotoObjAll' is also considered in the SQL query, in order to collect the corresponding photometric information. The detailed descriptions on the database 'PhotoObjAll' containing full photometric catalog quantities and on the database 'SpecObjall' containing all the spectroscopic information can be found in <https://skyserver.sdss.org/dr16/en/help/docs/tabledesc.aspx>. Furthermore, properties of the total stellar mass (the parameter `mstellar_median` and the corresponding uncertainty `mstellar_err`) will be discussed in Section 3, therefore, the SDSS public database of 'stellarMassPCAWiscM11' as described in detail in Maraston & Stromback (2011); Chen et al. (2012) is also considered in the SQL query.

Before proceeding further, spectroscopic features of the collected main galaxies are carefully checked, in order to measure emission lines after subtractions of the SSP method determined stellar continuum. In this manuscript, the commonly applied SSP (Simple Stellar Population) (Bruzual & Charlot 1993; Kauffmann et al. 2003b; Cid Fernandes et al. 2005, 2013; Lopez Fernandez et al. 2016; Cappellari 2017; Werle 2019) method is accepted to determine contributions of stellar lights in the SDSS spectra, with the 39 SSP templates discussed in Bruzual & Charlot (1993); Kauffmann et al. (2003b) which include the population age from 5Myr to 12Gyr with three solar metallicities ($Z = 0.008, 0.05, 0.02$). Through the Levenberg-Marquardt least-squares minimization method (the known MPFIT package, <https://pages.physics.wisc.edu/~craigm/idl/cmpfit.html>) (Markwardt 2009), sum of the strengthened, broadened and shifted SSP templates can be applied to describe the SDSS spectrum with emission lines being masked out by line width about 400km/s at zero intensity, similar as what we have recently done in Zhang et al. (2019); Zhang (2022b,c, 2023). Left panels of Fig. 1 show examples on the SSP method determined the best descriptions and the corresponding line spectrum of a Type-2 AGN SDSS 0533-51994-0031 (plate-mjd-fiberid). Here, line spectrum is calculated by the SDSS spectrum minus the SSP method determined stellar continuum.

After subtractions of the stellar continuum, emission lines can be described by Gaussian functions. Here, the narrow emission lines of H α , H β , [O III] λ 4959, 5007Å doublet and [N II] λ 6548, 6583Å doublet are mainly considered, in order to classify SDSS main galaxies by properties of the narrow emission line flux ratios in the BPT diagram of O3HB versus N2HA. Each Gaussian component is applied to describe each narrow emission line, besides the [O III] doublet which are described by core plus extended

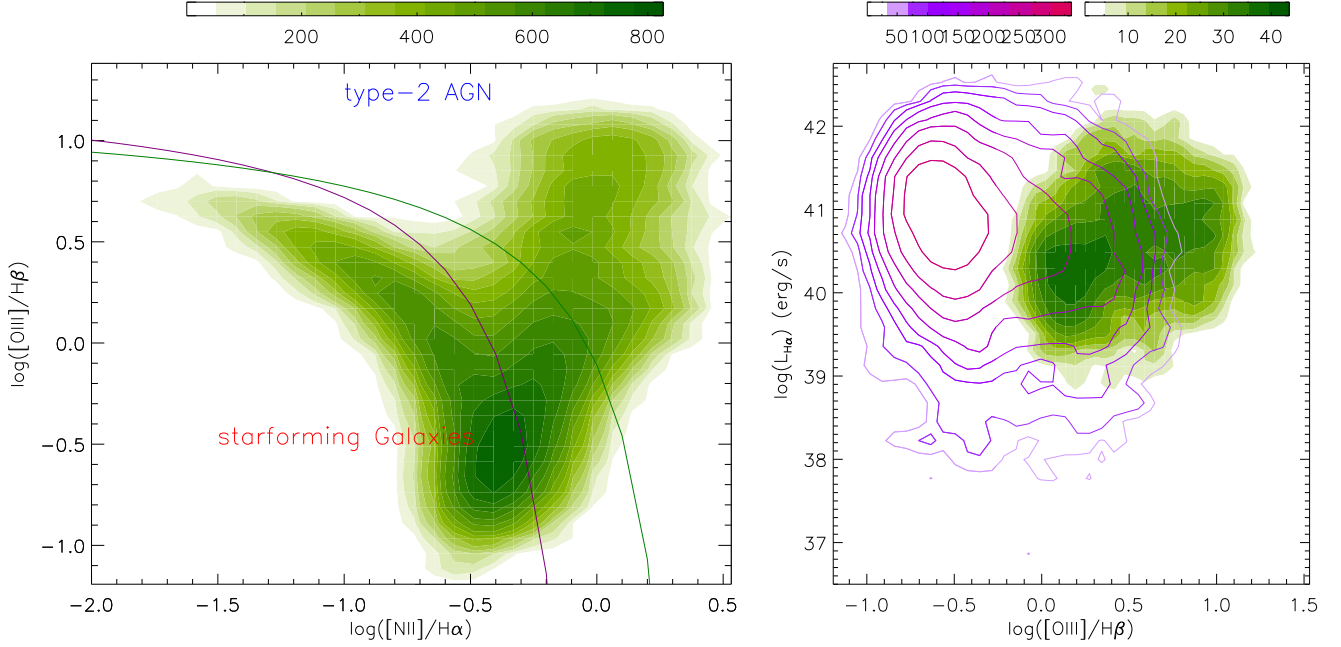


Figure 2. Left panel shows the BPT diagram of O3HB versus N2HA for all the narrow emission-line main galaxies collected from the SDSS DR16, with the collected 4112 Type-2 AGN lying above the dividing line shown as solid dark green line and the collected 19351 starforming galaxies lying below the dividing line shown as solid purple line. Right panel shows the dependence of $L_{H\alpha}$ on the parameter O3HB. In the right panel, the contour filled with greenish colors represents the results in the Type-2 AGN, and the contour with contour levels in reddish lines represents the results in the starforming galaxies. In each panel, the color bar is shown in the top region to represent the corresponding number densities related to different colors.

broad Gaussian components probably related to shifted wings (Greene & Ho 2005; Shen et al. 2011; Zhang 2021). Due to few effects of broad emission lines, there are no severe restrictions on the model parameters of each Gaussian component, besides the flux ratio of [O III] ([N II]) doublet fixed to the theoretical value of 3, and the emission line flux not smaller than zero. Then, through the Levenberg-Marquardt least-squares minimization method, the narrow emission lines can be measured. As examples, the right panels of Fig. 1 show the best-fitting results to the narrow emission lines in the line spectrum of the Type-2 AGN SDSS 0533-51994-0031 of which spectrum shown in the left panels. Here, one point should be noted. As shown in the example in Fig. 1, almost all the collected objects have their [N II] doublet and narrow Balmer lines to be described without considering extended components.

Based on the measured reliable line parameters¹, the main galaxies with reliable measurements of the narrow emission lines are collected, based on the criteria that each measured line parameter is at least five times larger than its corresponding measured uncertainty and that the flux ratio (Balmer decrement) of the narrow $H\alpha$ to the narrow $H\beta$ is less than 6 to ignore effects of serious obscuration on the following results.

Then, the well-known BPT diagram of O3HB versus N2HA is applied to classify the main galaxies into starforming galaxies and Type-2 AGN by the reported dividing lines in the literature (Kewley et al. 2019; Kauffmann et al. 2003; Zhang et al. 2020).

$$\begin{aligned} \log(O3HB) &= 0.61/(\log(N2HA) - 0.05) + 1.30 \quad (\text{green}) \\ \log(O3HB) &= 0.61/(\log(N2HA) - 0.47) + 1.19 \quad (\text{purple}) \end{aligned} \quad (2)$$

. As shown in the left panel of Fig. 2, there are 19351 main galaxies classified as starforming galaxies in the BPT diagram lying below the dividing line shown as solid purple line, and 4112 main galaxies classified as Type-2 AGN in the BPT diagram lying above the dividing line shown as solid dark green line. Based on the measured line parameters, the median Balmer decrement is 4.10 in the starforming galaxies and 4.18 in the Type-2 AGN, indicating not different obscuration effects on the following results.

¹ Actually, there is a SDSS provided databases 'GalSpecLine' (<https://skyserver.sdss.org/dr16/en/help/browser/browser.aspx?cmd=description+GalSpecLine+U>) including measured emission line parameters of all the main galaxies by MPA-JHU, as well described in Brinchmann et al. (2004); Tremonti (2004); Kauffmann et al. (2003a) and in https://www.sdss.org/dr15/spectro/galaxy_mpajhu/. The measured line parameters in this manuscript are well consistent with those in the databases 'GalSpecLine'. The same results can be found by applications of the line parameters in 'GalSpecLine'.

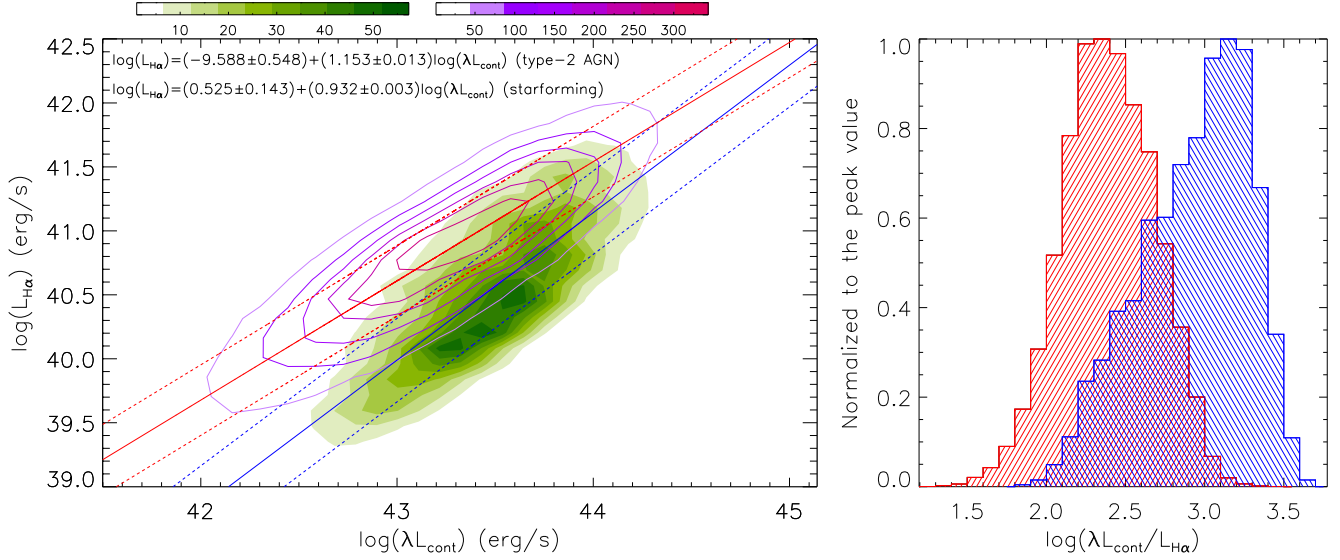


Figure 3. Left panel shows the correlation between $L_{H\alpha}$ and λL_{cont} in the 19351 starforming galaxies (the contour with contour levels in reddish colors) and in the 3836 Type-2 AGN (the contour filled with greenish colors). Right panel shows the distributions of $\log(R_{CL})$ in the starforming galaxies (filled with red lines) and in the Type-2 AGN (filled with blue lines). In the left panel, solid and dashed blue lines, solid and dashed red lines show the best-fitting results (the corresponding formula marked in the top-left corner) and the corresponding 1RMS scatters to the correlations in the Type-2 AGN and in the starforming galaxies, respectively.

Before ending the section, an additional point should be noted. Although the Type-2 AGN are collected from the SDSS pipeline classified main galaxies (with no expected broad emission lines), it is necessary to check whether there were any collected Type-2 AGN with probably broad emission lines and probably AGN continuum emissions included in the SDSS spectra. After subtractions of the stellar continuum, emission lines around $H\alpha$ (rest wavelength from 6200 to 6800Å) of all the collected 4112 Type-2 AGN have been re-measured by the narrow Gaussian functions applied to describe the narrow emission lines but by three additional broad Gaussian functions (second moment larger than 600km/s) applied to describe probably broad $H\alpha$. Based on the criterion that the measured parameters larger than 5 times of their corresponding uncertainties in one of the three broad Gaussian components in broad $H\alpha$, there are 285 Type-2 AGN with probably broad $H\alpha$. Therefore, there are 3836 (4121-285) Type-2 AGN in our final sample.

3. MAIN RESULTS AND DISCUSSIONS

Based on the measured line parameters and the continuum emission features of the collected 19351 starforming galaxies, there is a strong linear correlation between the narrow $H\alpha$ line luminosity ($L_{H\alpha}$) and the continuum luminosity at 5100Å (λL_{cont}) with the Spearman rank correlation coefficient of 0.88 ($P_{null} < 10^{-15}$). In this manuscript, although only objects are collected with flux ratio smaller than 6 of narrow $H\alpha$ to narrow $H\beta$, the $L_{H\alpha}$ and λL_{cont} have been reddening corrected for the objects with flux ratios of narrow $H\alpha$ to narrow $H\beta$ larger than 3.1, accepted 3.1 as the intrinsic flux ratio of narrow $H\alpha$ to narrow $H\beta$. After considering the uncertainties in both coordinates, the best fitting results shown in the left panel of Fig. 3 are determined through the Least Trimmed Squares (LTS) robust technique (Cappellari et al. 2013; Mahdi & Mohammad 2017),

$$\log\left(\frac{L_{H\alpha}}{\text{erg} \cdot \text{s}^{-1}}\right) = (0.525 \pm 0.143) + (0.932 \pm 0.003) \log\left(\frac{\lambda L_{cont}}{\text{erg} \cdot \text{s}^{-1}}\right) \quad (3)$$

The strong linear correlation in the starforming galaxies can be used as a standard candle to check effects of AGN feedback, by comparing the correlations of $L_{H\alpha}$ versus λL_{cont} between starforming galaxies and Type-2 AGN.

Based on the measured parameters of the Type-2 AGN, there is also a strong linear correlation between $L_{H\alpha}$ and λL_{cont} , with the Spearman rank correlation coefficient of 0.80 ($P_{null} < 10^{-15}$), also shown in the left panel of Fig. 3. Here, the $L_{H\alpha}$ and λL_{cont} are the reddening corrected values in the Type-2 AGN. After considering the uncertainties in both coordinates, the best-fitting results in the Type-2 AGN are determined by the LTS technique,

$$\log\left(\frac{L_{H\alpha}}{\text{erg} \cdot \text{s}^{-1}}\right) = (-9.588 \pm 0.548) + (1.153 \pm 0.013) \log\left(\frac{\lambda L_{cont}}{\text{erg} \cdot \text{s}^{-1}}\right) \quad (4)$$

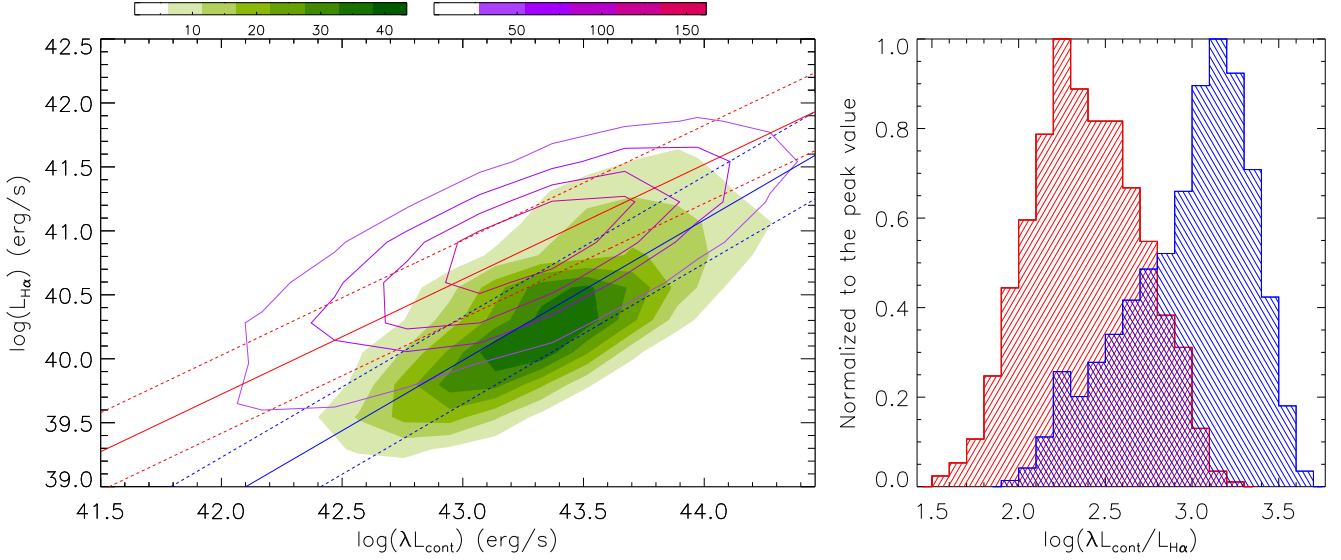


Figure 4. Same as Fig. 3, but for the starforming galaxies with $S/N > 30$ and the Type-2 AGN with $S/N > 30$.

It is clear that the linear correlations have much different intercepts but similar slopes between the Type-2 AGN and the starforming galaxies.

The expected $L_{H\alpha}$ are statistically smaller for given continuum luminosities in the Type-2 AGN than in the starforming galaxies. Right panel of Fig. 3 shows the distributions of luminosity ratio R_{CL} of λL_{cont} to $L_{H\alpha}$. The median values of $\log(R_{CL})$ are about 2.39 ± 0.29 and 2.99 ± 0.34 in the starforming galaxies and in the Type-2 AGN, respectively. Uncertainties of the median values are the standard deviations of the $\log(R_{CL})$. The student's T-statistic technique can be applied to confirm that the starforming galaxies and the Type-2 AGN have different mean values of $\log(R_{CL})$ with significance level higher than 5σ . Therefore, the different correlations between λL_{cont} and $L_{H\alpha}$ can be confirmed in the starforming galaxies and in the Type-2 AGN.

Before proceeding further, effects of signal-to-noise ratio (S/N) of SDSS spectra are simply discussed as follows on the shown results in Fig. 3 for the starforming galaxies with $S/N > 20$ and the Type-2 AGN with $S/N > 20$. Among the starforming galaxies and the Type-2 AGN, the 2957 starforming galaxies with $S/N > 30$ and the 1060 Type-2 AGN with $S/N > 30$ are collected to re-check the correlation between $L_{H\alpha}$ versus λL_{cont} , shown in Fig. 4. The linear correlations can be confirmed with the Spearman rank correlation coefficients of about 0.84 ($P_{null} < 10^{-15}$) and 0.79 ($P_{null} < 10^{-15}$) for the starforming galaxies with $S/N > 30$ and for the Type-2 AGN with $S/N > 30$, respectively. And the best fitting results can be described as

$$\begin{aligned} \log\left(\frac{L_{H\alpha}}{\text{erg} \cdot \text{s}^{-1}}\right) &\propto 0.898 \log\left(\frac{\lambda L_{cont}}{\text{erg} \cdot \text{s}^{-1}}\right) \quad (\text{star forming}) \\ \log\left(\frac{L_{H\alpha}}{\text{erg} \cdot \text{s}^{-1}}\right) &\propto 1.098 \log\left(\frac{\lambda L_{cont}}{\text{erg} \cdot \text{s}^{-1}}\right) \quad (\text{AGN}) \end{aligned} \quad (5)$$

The median values and the corresponding standard deviations (as uncertainties) of $\log(R_{CL})$ are about 2.37 ± 0.31 and 3.04 ± 0.35 in the 2957 starforming galaxies with $S/N > 30$ and in the 1060 Type-2 AGN with $S/N > 30$, respectively. And the student's T-statistic technique can be applied to confirm the different mean values of $\log(R_{CL})$ with significance level higher than 5σ . The similar results as those shown in Fig. 3 strongly indicate few effects of S/N on our final results. Therefore, there are no further discussions on effects of S/N .

Considering the strong connections between starforming properties and narrow $H\alpha$ line luminosities, effects of AGN feedback on narrow $H\alpha$ line luminosity in Type-2 AGN can be expected. If there was positive AGN Feedback on starforming, statistically stronger narrow $H\alpha$ emissions could be expected in the Type-2 AGN than in the starforming galaxies, otherwise, negative AGN feedback should lead to statistically weaker narrow $H\alpha$ emissions in the Type-2 AGN. Based on the results in Fig. 3, there are weaker narrow $H\alpha$ emissions (larger values of R_{CL}) in the Type-2 AGN than in the starforming galaxies. Therefore, the results in Fig. 3 can be accepted as apparent clues to support negative AGN feedback in the local Type-2 AGN in SDSS, considering the continuum emissions with few contaminations of central AGN activity in host galaxies of Type-2 AGN.

In order to confirm the shown results in Fig. 3 leading to negative AGN feedback, the following effects are mainly considered.

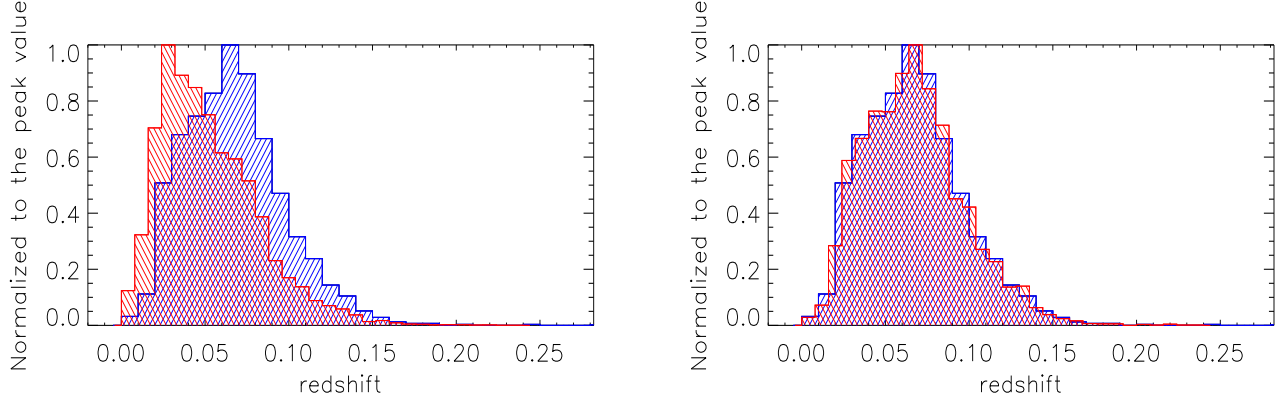


Figure 5. Left panel shows the redshift distributions of the collected 19351 starforming galaxies (filled with red lines) and the collected 3836 Type-2 AGN (filled with blue lines). Right panel shows the redshift distributions of the randomly re-collected 7672 starforming galaxies (filled with red lines) in the subsample and the 3836 Type-2 AGN (filled with blue lines).

If the lower line intensities of intrinsic narrow $H\alpha$ in Type-2 AGN was not due to the negative AGN Feedback but due to central AGN activity, it will be necessary to check whether stronger AGN activity can lead to lower line intensities of intrinsic narrow $H\alpha$. If lower line intensities of intrinsic narrow $H\alpha$ in Type-2 AGN were actually due to stronger AGN activity, statistically lower $L_{H\alpha}$ for given λL_{cont} could be expected in Type-2 AGN. However, in the collected Type-2 AGN, after checking the dependence of narrow $H\alpha$ luminosity on central AGN activity traced by the narrow emission line ratio of O3HB, one positive correlation can be found with the Spearman rank correlation coefficient of 0.31 ($P_{null} < 10^{-15}$), shown in the right panel of Fig. 2. Meanwhile, in the collected starforming galaxies, there is a weak negative dependence of $L_{H\alpha}$ on the parameter of O3HB, with the Spearman rank correlation coefficient of -0.22 ($P_{null} < 10^{-15}$), also shown in the right panel of Fig. 2. Therefore, the observed lower $L_{H\alpha}$ in Type-2 AGN is not due to stronger central AGN activity.

Furthermore, effects of the different redshift distributions are considered on the results shown in Fig. 3 between the starforming galaxies and the Type-2 AGN. Left panel of Fig. 5 shows the redshift distributions of the 19351 starforming galaxies with median z about 0.047 ± 0.029 and the 3836 Type-2 AGN with median z about 0.065 ± 0.030 . Uncertainties of the median values are the standard deviations of z . And the student's T-statistic technique can be applied to confirm that the median values of z are different with significance level higher than 5σ . Besides the different median redshifts, through the two-sided Kolmogorov-Smirnov statistic technique, the starforming galaxies and the Type-2 AGN have the same redshift distributions with significance level smaller than 10^{-15} . Therefore, it is necessary to check effects of the different redshift distributions on the results shown in Fig. 3. In order to ignore the effects of the different redshift distributions, the simplest method is to check the results shown in Fig. 3 but for two samples of starforming galaxies and Type-2 AGN which have the same redshift distributions.

Based on the redshift distributions of the starforming galaxies and the Type-2 AGN, 7672 starforming galaxies are easily and randomly collected into one subsample, which has the similar redshift distribution as that of the sample of the 3836 Type-2 AGN, as the results shown in the right panel of Fig. 5. Through the two-sided Kolmogorov-Smirnov statistic technique, the subsample of the 7672 starforming galaxies and the 3836 Type-2 AGN have the same redshift distributions with significance level higher than 99.99%. Then, the correlation between $L_{H\alpha}$ and λL_{cont} is shown in the left panel of Fig. 6 for the subsample of the 7672 starforming galaxies. The linear correlation can be confirmed with the Spearman rank correlation coefficient of about 0.88 ($P_{null} < 10^{-15}$) for the re-collected 7672 starforming galaxies in the subsample. And the LTS technique determined best fitting results are shown in the left panel of Fig. 6 with the corresponding formula marked in the top region of the left panel of Fig. 6. It is clear that the lower expected $L_{H\alpha}$ for given λL_{cont} can be re-confirmed in the Type-2 AGN than in the starforming galaxies in the subsample, as shown in the right panel of Fig. 6 with the median values and the corresponding standard deviations of $\log R_{CL}$ about 2.40 ± 0.28 and 2.99 ± 0.34 in the 7672 starforming galaxies in the subsample and in the 3836 Type-2 AGN, respectively. And the student's T-statistic technique can be applied to confirm the different median values of $\log R_{CL}$ with significance level higher than 5σ . Therefore, the very different correlations between $L_{H\alpha}$ and λL_{cont} are intrinsic and reliable between the starforming galaxies and the Type-2 AGN, after considering effects of different z distributions of the starforming galaxies and the Type-2 AGN.

Furthermore, combining with aperture effects, effects of the different distributions of total stellar mass M_T and different host galaxy morphologies are considered on the results shown in Fig. 3 between the starforming galaxies and the Type-2 AGN. Left

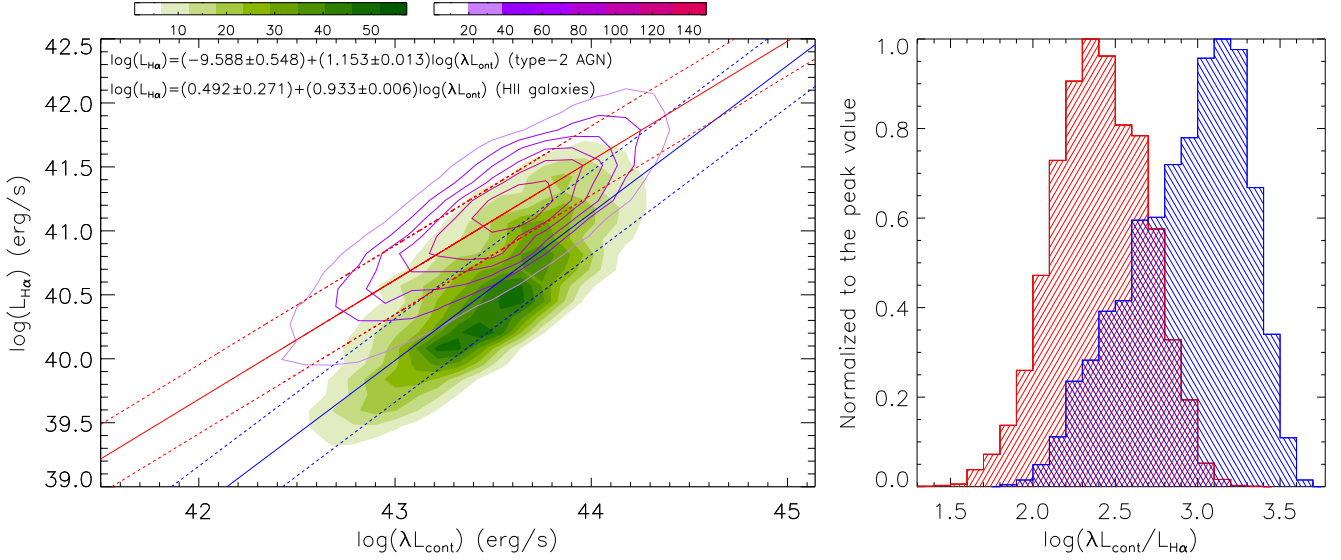


Figure 6. Similar as Fig. 3, but the starforming galaxies are the re-collected 7672 starforming galaxies in the subsample.

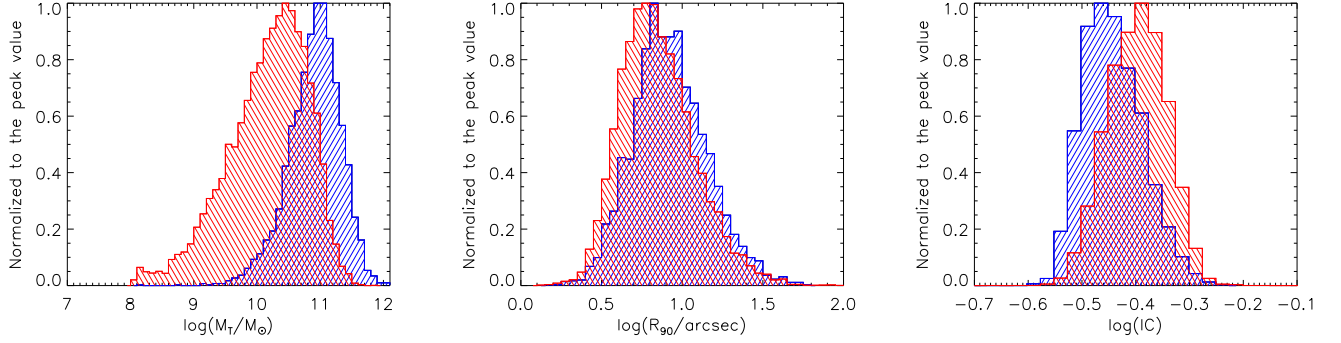


Figure 7. Left panel shows the $\log(M_T)$ distributions of the collected 18995 starforming galaxies (filled with red lines) and the collected 3827 Type-2 AGN (filled with blue lines). Middle and right panel show the distributions of the R_{90} and IC of the 18131 starforming galaxies and the 3652 Type-2 AGN with reliable measurements of parameters of petroR90_r and petroR50_r.

panel of Fig. 7 shows the M_T distributions of the 18995 starforming galaxies (356 starforming galaxies not included, due to their total stellar masses smaller than five times of their corresponding uncertainties) with median $\log(M_T/M_\odot)$ about 10.26 ± 0.63 and of the 3827 Type-2 AGN (36 Type-2 AGN not included, due to their total stellar masses smaller than five times of their corresponding uncertainties) with median $\log(M_T/M_\odot)$ about 10.94 ± 0.41 . Uncertainties of the median values are the standard deviations of $\log(M_T/M_\odot)$. And the student's T-statistic technique can be applied to confirm that the median values of $\log(M_T)$ are different with significance level higher than 5σ . And, through the two-sided Kolmogorov-Smirnov statistic technique, the starforming galaxies and the Type-2 AGN have the same redshift distributions with significance level smaller than 10^{-15} . Therefore, it is necessary to check effects of the different M_T distributions on the results shown in Fig. 3.

Meanwhile, middle panel of Fig. 7 shows the R_{90} (as the radii containing 90% of the Petrosian flux in SDSS r band²) distributions of the 18131 starforming galaxies (1219 starforming galaxies not included, due to their petroR90_r smaller than five times of their corresponding uncertainties) with median $\log(R_{90}/arcsec)$ about 0.83 ± 0.23 and of the 3652 Type-2 AGN (184 Type-2 AGN not included, due to their petroR90_r smaller than five times of their corresponding uncertainties) with median $\log(R_{90}/arcsec)$ about 0.91 ± 0.22 . Uncertainties of the median values are the standard deviations of $\log(R_{90}/arcsec)$. And the student's T-statistic

² The same results can be found, if the Petrosian radius applied in the other bands.

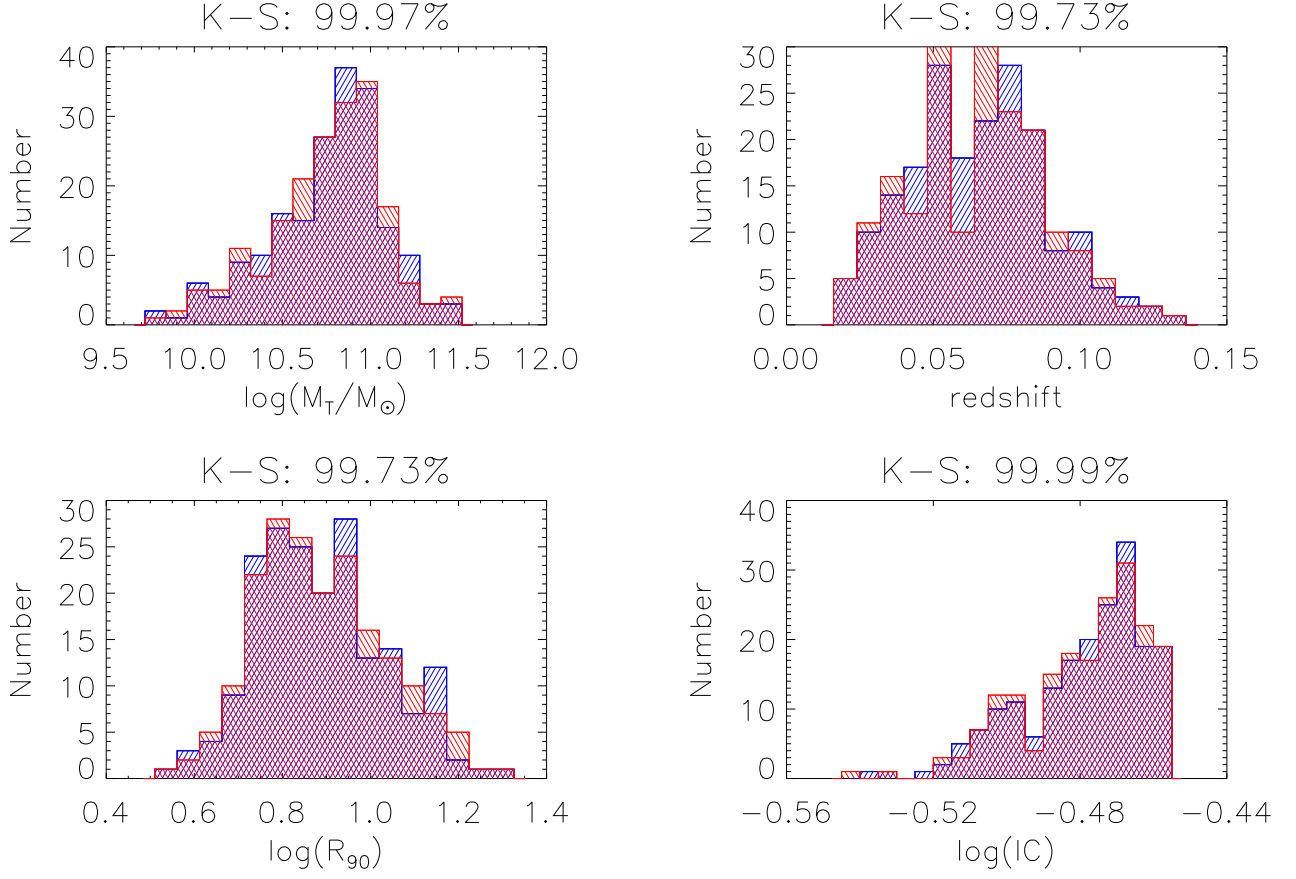


Figure 8. Distributions of the M_T (top left panel), z (top right panel), R_{90} (bottom left panel) and IC (bottom right panel) of the 191 starforming galaxies and the 191 Type-2 AGN in the subsamples with the same distributions of M_T , z , R_{90} and IC ($IC < 0.35$ and $dehav_r$ larger than 0.8). In each panel, histogram filled with red lines shows the results for the starforming galaxies, histogram filled with blue lines shows the results for the Type-2 AGN.

technique can be applied to confirm that the median values of $\log(R_{90})$ are different with significance level higher than 5σ . And, through the two-sided Kolmogorov-Smirnov statistic technique, the starforming galaxies and the Type-2 AGN have the same R_{90} distributions with significance level smaller than 10^{-15} . Therefore, it is necessary to check effects of the different R_{90} distributions on the results shown in Fig. 3.

Meanwhile, right panel of Fig. 7 shows the distributions of the inverse concentration parameter (Shimasaku et al. 2001; Strateva et al. 2001) $IC = R_{50}/R_{90}$ (where R_{50} and R_{90} as the radii containing 50% and 90% of the Petrosian flux in SDSS r band³) of the 18131 starforming galaxies (with reliable measurements of $petroR90_r$ and $petroR50_r$) and the 3652 Type-2 AGN (with reliable measurements of $petroR90_r$ and $petroR50_r$). The median values of $\log(IC)$ are about -0.39 ± 0.05 and -0.45 ± 0.06 for the starforming galaxies and the Type-2 AGN, respectively. And the student's T-statistic technique can be applied to confirm that the median values of $\log(IC)$ are different with significance level higher than 5σ . And, through the two-sided Kolmogorov-Smirnov statistic technique, the starforming galaxies and the Type-2 AGN have the same IC distributions with significance level smaller than 10^{-15} . Therefore, it is necessary to check effects of the different IC distributions on the results shown in Fig. 3.

In order to check effects of different distributions of z , M_T , R_{90} and IC , a simple method can be considered as follows by re-collected starforming galaxies and Type-2 AGN into new subsamples which have the same distributions of z , M_T , R_{90} and IC . The same distributions of z and R_{90} can be applied to ignore aperture effects on the results for the objects in the subsamples. The same distribution of M_T can be applied to ignore effects of different total stellar mass on the results for the objects in the

³ The same results can be found, if the Petrosian radius applied in the other bands.

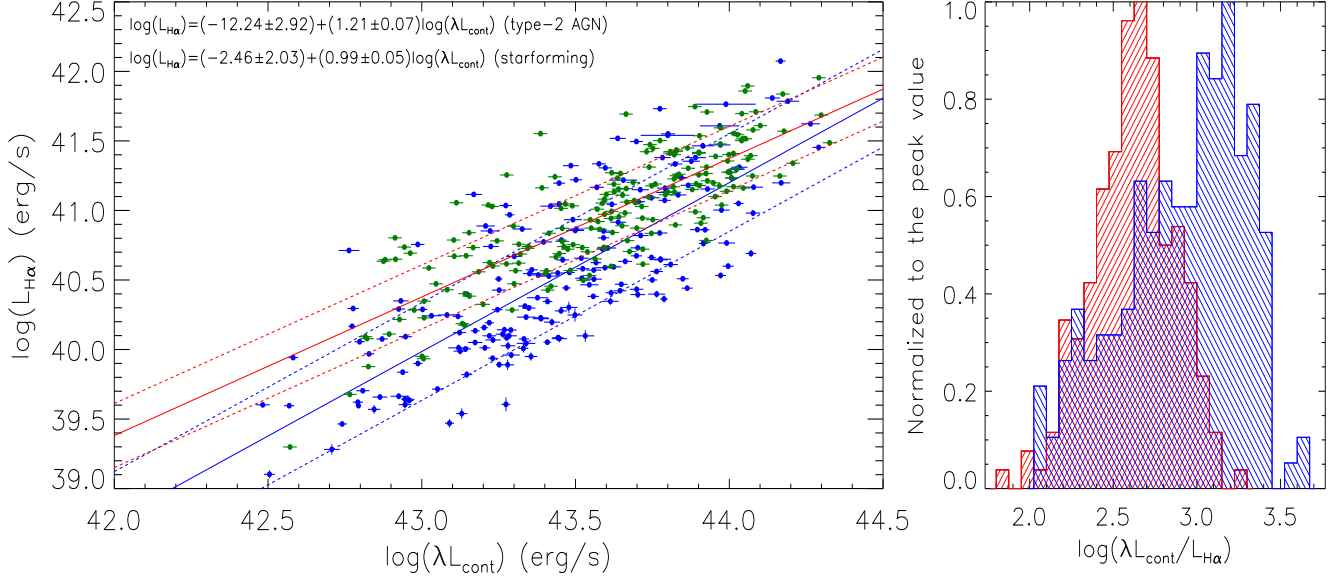


Figure 9. Similar as Fig. 3 and as Fig. 6, but for the re-collected 191 starforming galaxies and the re-collected 191 Type-2 AGN in the subsamples which have the same distributions of M_T , z , q_0 and IC ($IC < 0.35$ and $devab_r$ larger than 0.8). In the left panel, solid circles plus error bars in blue show the results for the 191 Type-2 AGN, and circles plus error bars in dark green show the results for the 191 starforming galaxies.

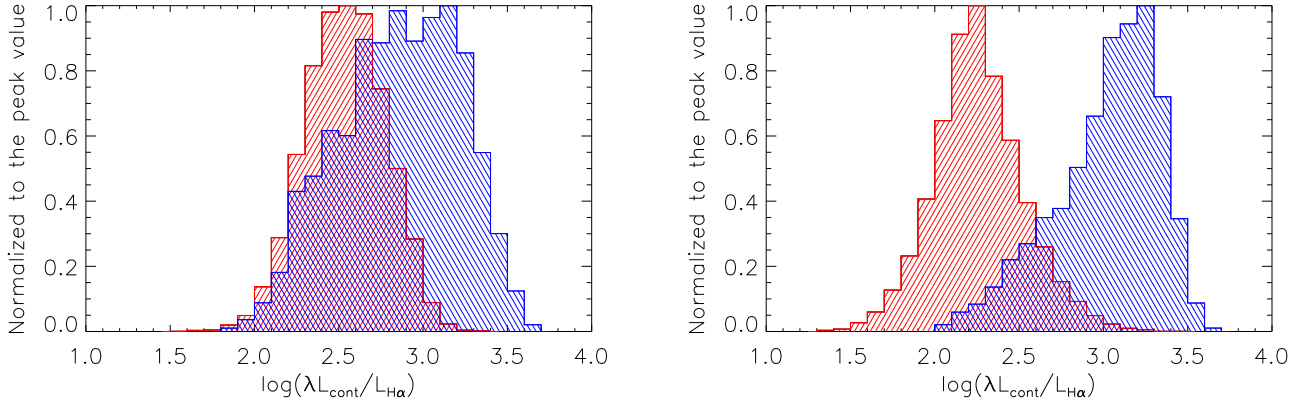


Figure 10. Left panel shows the distributions of $\log R_{CL}$ of the starforming galaxies in the SF_H sample and the Type-2 AGN in the AGN_L sample. Right panel shows the distributions of $\log R_{CL}$ of the starforming galaxies in the SF_L sample and the Type-2 AGN in the AGN_H sample. In each panel, histogram filled with dark green lines shows the results for the starforming galaxies, histogram filled with blue lines shows the results for the Type-2 AGN.

subsamples. And the same distributions of $IC < 0.35$ (combining with $devab_r$ larger than 0.8) can be applied to simply accepted that the host galaxies of the re-collected objects are elliptical galaxies as discussed in Shimasaku et al. (2001); Strateva et al. (2001) and in <https://www.sdss4.org/dr16/algorithms/classify/>, in order to ignore effects of inclinations of disk galaxies and/or to ignore probable effects of different morphologies. Based on the z distributions (shown in the left panel of Fig. 5) and the distributions of M_T , R_{90} and IC shown in Fig. 7 of the starforming galaxies and the Type-2 AGN, a subsample of 191 starforming galaxies and a subsample of 191 Type-2 AGN can be collected, with the two subsamples having the same distributions of z , M_T , R_{90} and IC , which are shown in Fig. 8. Through the two-sided Kolmogorov-Smirnov statistic technique, the subsample of the 191 starforming galaxies and the subsample of the 191 Type-2 AGN have the same distributions of z , M_T , R_{90} and IC , with significance levels higher than 99.5%.

Then, the correlations between $L_{H\alpha}$ and λL_{cont} are shown in the left panel of Fig. 9 for the 191 starforming galaxies and the 191 Type-2 AGN in the subsamples which have the same distributions of z , M_T , R_{90} and IC . And the mean ratio of emission line flux

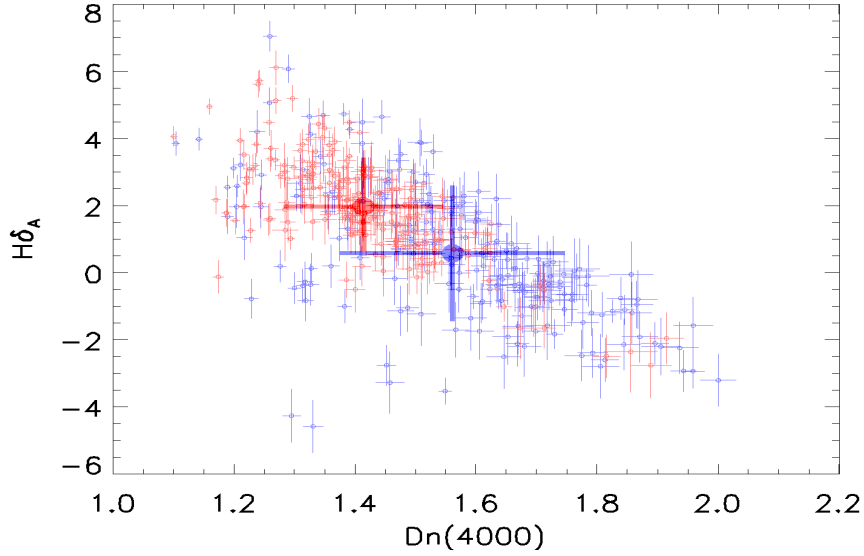


Figure 11. On the properties of $Dn(4000)$ and $H\delta_A$ in the 191 starforming galaxies (open circles plus error bars in red) and the 191 Type-2 AGN (open circles plus error bars in blue) in the subsamples with the same distributions of z , M_T , R_{90} and IC ($IC < 0.35$ and $devab_r$ larger than 0.8). Solid circles plus error bars in red and in blue show the mean positions and the corresponding uncertainties (the standard deviation) of the starforming galaxies and the Type-2 AGN, respectively.

to its corresponding uncertainty is about 36 in narrow $H\alpha$, the mean ratio of continuum emission intensity to its corresponding uncertainty is about 21. The linear correlations can be confirmed with the Spearman rank correlation coefficients of about 0.83 ($P_{null} < 10^{-15}$) for the re-collected 191 starforming galaxies in the subsample and of about 0.78 ($P_{null} < 10^{-15}$) for the re-collected 191 Type-2 AGN in the subsample. And the LTS technique determined best fitting results are shown in the left panel of Fig. 9 with the corresponding formula marked in the top region of the left panel of Fig. 9. It is clear that the lower expected $L_{H\alpha}$ for given λL_{cont} can be re-confirmed in the Type-2 AGN than in the starforming galaxies in the subsamples, as shown in the right panel of Fig. 9 with the median values and the corresponding standard deviations of $\log R_{CL}$ about 2.61 ± 0.24 and 2.98 ± 0.36 in the 191 starforming galaxies and the 191 Type-2 AGN in the subsamples, respectively. And the student's T-statistic technique can be applied to confirm the different median values of $\log R_{CL}$ with significance levels higher than 5σ . Therefore, even after considering effects of different distributions of z , M_T , R_{90} and IC , the very different correlations between $L_{H\alpha}$ and λL_{cont} are intrinsic and reliable between the starforming galaxies and the Type-2 AGN.

Moreover, due to unconfirmed positive or negative AGN feedback on starforming histories, the following extreme comparisons can be checked between starforming galaxies with lower (higher) total stellar masses and Type-2 AGN with higher (lower) total stellar masses. Among the 18995 starforming galaxies with median $\log(M_T/M_\odot)$ about 10.26, there are half of the starforming galaxies in SF_H sample with total stellar masses $\log(M_T/M_\odot)$ larger than the median value 10.26, and the other half of the starforming galaxies in SF_L sample with total stellar masses $\log(M_T/M_\odot)$ smaller than the median value 10.26. Meanwhile, among the 3836 Type-2 AGN with median $\log(M_T/M_\odot)$ about 10.94, there are half of the Type-2 AGN in AGN_H sample with total stellar masses $\log(M_T/M_\odot)$ larger than the median value 10.94, and the other half of the Type-2 AGN in AGN_L sample with total stellar masses $\log(M_T/M_\odot)$ smaller than the median value 10.94. Then, left panel of Fig. 10 shows the distributions of $\log R_{CL}$ of the 9478 starforming galaxies in the SF_H sample with median $\log R_{CL}$ about 2.53 ± 0.24 and the 1918 Type-2 AGN in the AGN_L sample with median $\log R_{CL}$ about 2.88 ± 0.35 , right panel of Fig. 10 shows the distributions of $\log R_{CL}$ of the 9477 starforming galaxies in the SF_L sample with median $\log R_{CL}$ about 2.25 ± 0.26 and the 1918 Type-2 AGN in the AGN_L sample with median $\log R_{CL}$ about 3.07 ± 0.30 . And the student's T-statistic technique can be applied to confirm the different median values of $\log R_{CL}$ shown in Fig. 10 with significance levels higher than 5σ . Therefore, the very different correlations between $L_{H\alpha}$ and λL_{cont} are intrinsic and reliable between the starforming galaxies and the Type-2 AGN, even after considering very different M_T distributions of the starforming galaxies and the Type-2 AGN.

Moreover, the parameters of $Dn(4000)$ and $H\delta_A$ (Balogh et al. 1999; Worthey & Ottaviani 1997) are compared between the 206 starforming galaxies and the 206 Type-2 AGN in the subsamples with the same distributions of z , M_T , R_{90} and IC ($IC < 0.35$ and $devab_r$ larger than 0.8), because the two parameters can provide intrinsic information on stellar ages (Kauffmann et al. 2003).

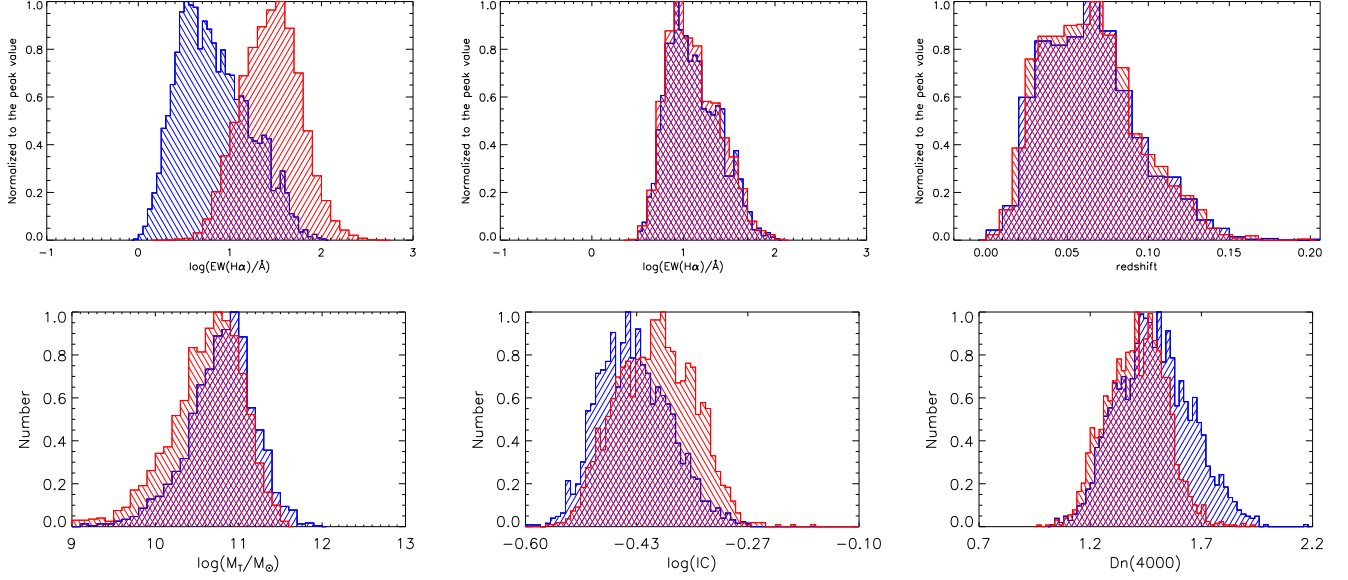


Figure 12. Top left panel shows the Distributions of $EW(H\alpha)$ of the starforming galaxies and the Type-2 AGN. Top middle panel and top right panel show the distributions of redshift and $EW(H\alpha)$ of the starforming galaxies and the Type-2 AGN in the subsamples which have the same distributions of z and $EW(H\alpha)$. Bottom panels show the distributions of M_T , IC and $Dn(4000)$ of the starforming galaxies and the Type-2 AGN in the subsamples which have the same distributions of z and $EW(H\alpha)$. In each panel, histogram filled with red lines shoes the results for the starforming galaxies, and histogram filled with blue lines are for the Type-2 AGN.

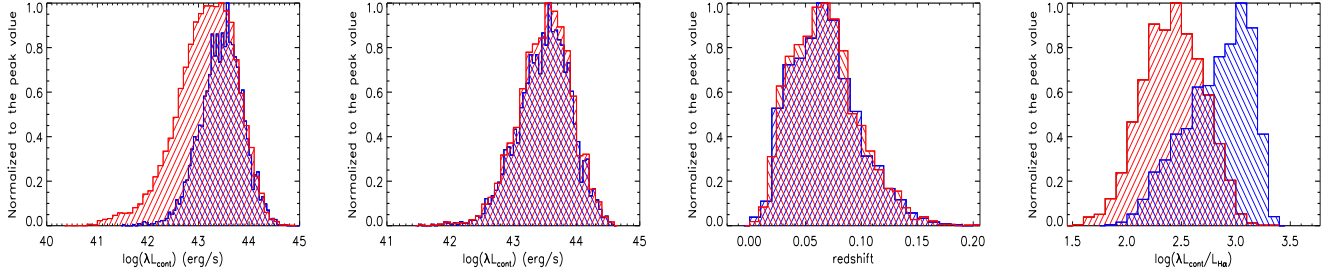


Figure 13. Left panel shows the Distributions of λL_{cont} of the starforming galaxies and the Type-2 AGN. The second panel and the third panel show the distributions of redshift and λL_{cont} of the starforming galaxies and the Type-2 AGN in the subsamples which have the same distributions of z and λL_{cont} . Right panel shows the $\log(R_{CL})$ distributions of the starforming galaxies and the Type-2 AGN in the subsamples which have the same distributions of z and λL_{cont} . In each panel, histogram filled with red lines shoes the results for the starforming galaxies, and histogram filled with blue lines are for the Type-2 AGN.

Here, the parameters $Dn(4000)$ and $H\delta_A$ are measured through the spectroscopic features similar as what have been done in [Kauffmann et al. \(2003\)](#). The results on $Dn(4000)$ and $H\delta_A$ are shown in Fig. 11. Median values and the corresponding standard deviations of $Dn(4000)$ and $H\delta_A$ are 1.57 ± 0.17 and 0.24 ± 0.02 in the 206 Type-2 AGN in the subsample, and 1.41 ± 0.13 and 1.99 ± 1.45 in the 206 starforming galaxies in the subsample, indicating older stellar populations in the host galaxies in the Type-2 AGN. And the student's T-statistic technique can be applied to confirm that the mean values of $Dn(4000)$ ($H\delta_A$) are different with significance levels higher than 5σ , between the starforming galaxies and the Type-2 AGN in the subsamples with the same distributions of z , M_T , R_{90} and IC ($IC < 0.35$ and $devab_r$ larger than 0.8). If there were positive AGN feedback on starforming in the host galaxies of Type-2 AGN, younger stellar ages should be clearly expected. Therefore, the results shown in Fig. 11 can be accepted as indirect evidence to support the globally negative AGN feedback on starforming.

Furthermore, as discussed in [Cid Fernandes et al. \(2011\)](#) that the Type-2 AGN and the starforming galaxies can be separated in the space of $EW(H\alpha)$ (equivalent width of narrow $H\alpha$) and $N2HA$, therefore it is necessary to check whether the different R_{CL} are only due to very different distributions of $EW(H\alpha)$ between the starforming galaxies and the Type-2 AGN. Top left panel of Fig. 12 shows the $\log(EW(H\alpha))$ distributions, with mean value of about 1.45 ± 0.32 for the starforming galaxies and of about

0.83 ± 0.38 for the Type-2 AGN. Then, based on the $EW(H\alpha)$ and redshift distributions, one subsample including 2013 starforming galaxies and one subsample including 2013 Type-2 AGN are created, with the same distributions of z and $EW(H\alpha)$ as shown in the top middle panel and the top right panel of Fig. 12. Through the two-sided Kolmogorov-Smirnov statistic technique, the two subsamples have the same distributions of z and $EW(H\alpha)$ with significance levels higher than 99.99%. Here, due to the same $EW(H\alpha)$ distributions for the 2013 Type-2 AGN and the 2013 HII galaxies in the subsamples, the similar dependence of $L_{H\alpha}$ on continuum luminosity can be expected, because both the $EW(H\alpha)$ and the linear dependence of $L_{H\alpha}$ on continuum luminosity have the same physical meanings. However, if there were no effects of AGN feedback on host galaxy properties of Type-2 AGN, similar host galaxy properties could be expected between the 2013 Type-2 AGN and the 2013 HII galaxies in the subsamples. Nevertheless, through the shown distributions of M_T , IC and $Dn(4000)$ of the objects in the subsamples in bottom panels of Fig. 12, there are very different host galaxy properties between the starforming galaxies and the Type-2 AGN in the subsamples. The mean values of $\log(M_T/M_\odot)$, $\log(IC)$ and $Dn(4000)$ are about 10.78 ± 0.41 , -0.44 ± 0.05 and 1.49 ± 0.16 for the 2013 Type-2 AGN in the subsample, and about 10.56 ± 0.54 , -0.40 ± 0.06 and 1.41 ± 0.13 for the 2013 starforming galaxies in the subsample. And the student's T-statistic technique can be applied to confirm that the mean values of host galaxy properties are different enough with significance levels higher than 5σ . And through the two-sided Kolmogorov-Smirnov statistic technique, the significance levels smaller than 10^{-15} for the objects in the subsamples having the same distributions of M_T , IC and $Dn(4000)$. In one word, besides the different $EW(H\alpha)$ distributions, AGN feedback could play the key role leading to the different R_{CL} .

Meanwhile, as shown above on the steeper dependence of $L_{H\alpha}$ and λL_{cont} in the Type-2 AGN, it is necessary to check whether more luminous Type-2 AGN included in our final sample can affect the statistical results on R_{CL} . Left panel of Fig. 13 shows the $\log(\lambda L_{cont}/(\text{erg/s}))$ distributions with the mean value of about 43.15 ± 0.59 for the starforming galaxies and of about 43.45 ± 0.42 for the Type-2 AGN. Then, based on the $\log(\lambda L_{cont})$ and redshift distributions, one subsample including 2967 starforming galaxies and one subsample including 2967 Type-2 AGN are created, with the same distributions of z and $\log(\lambda L_{cont})$ as shown in the second panel and the third panel of Fig. 13. Through the two-sided Kolmogorov-Smirnov statistic technique, the two subsamples have the same distributions of z and $\log(\lambda L_{cont})$ with significance levels higher than 99.99%. Then, right panel of Fig. 13 shows the distributions of $\log(R_{CL})$, with the mean value of about 2.42 ± 0.28 for the starforming galaxies and of about 2.83 ± 0.29 for the Type-2 AGN in the subsamples. And the student's T-statistic technique can be applied to confirm that the mean values of $\log(R_{CL})$ are different enough with significance levels higher than 5σ . In one word, more luminous Type-2 AGN cannot be applied to explain the apparent different $\log(R_{CL})$ between the starforming galaxies and the Type-2 AGN.

Certainly, in this manuscript, it has been accepted that there are no contribution of central AGN emissions to continuum emissions of host galaxies of Type-2 AGN. If considering the AGN contributions to continuum emissions leading to the different correlations between $L_{H\alpha}$ and λL_{cont} in the starforming galaxies and in the Type-2 AGN, about 58% of continuum emissions from central AGN activity could be expected in Type-2 AGN. So larger contributions should indicate stronger power law continuum emission components in SDSS spectra of Type-2 AGN. However, after checking SDSS spectra of the Type-2 AGN, there are no broad emission lines nor power law continuum components detected in SDSS spectra of Type-2 AGN. The flux-weighted mean spectrum of Type-2 AGN is shown in Fig. 14, which can be described by pure stellar templates without considerations of power law components, and have no apparent broad emission lines, to simply support that only small number of Type-2 AGN have broad emission lines and AGN continuum emissions included in the SDSS spectra. Furthermore, if there were strong contributions of central AGN activity to continuum emissions in host galaxies of Type-2 AGN, the calculated $H\delta_A$ could be about 2 times different from the shown results in left panel of Fig. 11 in the Type-2 AGN, leading to unexpected quite different correlations between $Dn(4000)$ and $H\delta_A$ in starforming galaxies and in host galaxies of Type-2 AGN.

4. SUMMARY AND CONCLUSIONS

The final summary and conclusions are as follows.

- Among all the low-redshift narrow emission line main galaxies in SDSS DR16 with $S/N > 20$, the spectroscopic narrow emission lines of $H\beta$, $[O\ III]$, $H\alpha$ and $[N\ II]$ are well measured, after subtractions of host galaxy contributions determined by the SSP method applied with 39 stellar templates.
- Based on the dividing lines applied in the BPT diagram of O3HB versus N2HA, 19531 starforming galaxies and 4112 Type-2 AGN are collected with reliable narrow emission lines.
- Based on the reliable measured parameters of the 19531 starforming galaxies, a strong linear correlation can be confirmed between the narrow $H\alpha$ line luminosity and the continuum luminosity at 5100\AA , with no contributions of AGN activity. The correlation in starforming galaxies can be treated as a standard candle.

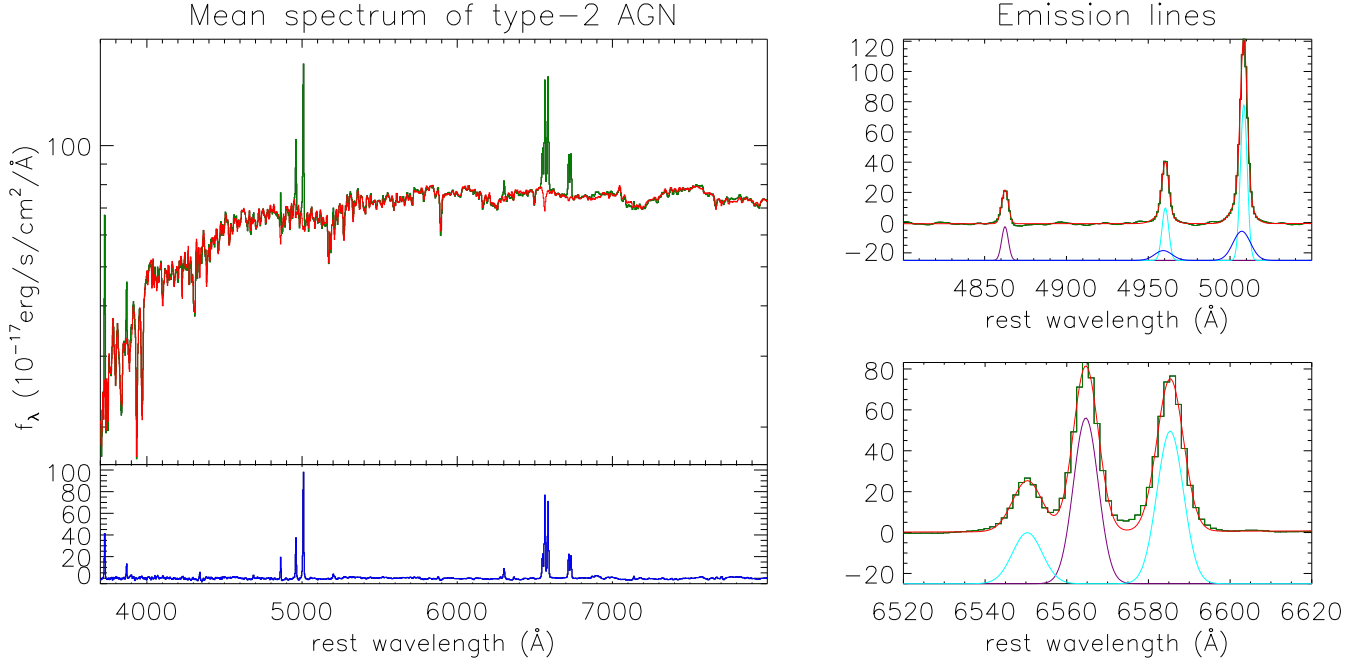


Figure 14. The mean spectrum of the Type-2 AGN. The results are the same as those shown in Fig. 1, but for the flux-weighted mean spectrum of the 4112 Type-2 AGN.

- Based on the reliable measured parameters of the 4112 Type-2 AGN, a strong correlation can be confirmed between the narrow $H\alpha$ line luminosity and the continuum luminosity at 5100\AA , however with quite different intercept from the correlation in the starforming galaxies.
- Starforming galaxies (Type-2 AGN) with $S/N > 30$ can lead to similar correlation between narrow $H\alpha$ line luminosity and continuum luminosity as those of starforming galaxies (Type-2 AGN) with $S/N > 30$, leading to few effects of spectral signal-to-noise on the final results.
- Statistically lower narrow $H\alpha$ line luminosities with significance level higher than 5σ can be confirmed for given continuum luminosities in the Type-2 AGN than in the starforming galaxies, lead to apparent clues to support globally negative AGN feedback in Type-2 AGN, even after considering effects of central AGN activity on narrow $H\alpha$ line luminosities, and effects of different distributions of redshift z , total stellar mass M_T , Petrosian radius R_{90} and inverse concentration parameter IC .
- Different host galaxy properties can be confirmed with significance levels higher than 5σ between the starforming galaxies and the Type-2 AGN in the subsamples which have the same distributions of redshift and $EW(H\alpha)$. Therefore, besides the different $EW(H\alpha)$ properties, AGN feedback could be the key role leading to the statistically lower narrow $H\alpha$ line luminosities for given continuum luminosities in the Type-2 AGN than in the starforming galaxies.
- Comparing properties of $Dn(4000)$ and inverse concentration parameter IC between the 206 starforming galaxies and the 206 Type-2 AGN in the final subsamples with the same distributions of z , M_T , R_{90} and IC ($IC < 0.35$ and $devab_r$ larger than 0.8), statistically older stellar ages in the Type-2 AGN can provide indirect evidence to support negative AGN feedback in local Type-2 AGN.
- Under the extreme assumption of no contributions of central AGN activity in the observed narrow $H\alpha$ in Type-2 AGN, the globally lower limited value can be estimated that more than 50% of narrow $H\alpha$ emissions have been suppressed in the host galaxies of the local SDSS Type-2 AGN due to globally negative AGN feedback.

1 Zhang gratefully acknowledge the anonymous referee for giving us constructive comments and suggestions to greatly improve
 2 the paper. Zhang gratefully thanks the kind financial support from GuangXi University and the kind grant supports from NSFC-
 3 12173020 and NSFC-12373014. This manuscript has made use of the data from the SDSS projects. The SDSS-III web site is
 4 <http://www.sdss3.org/>. SDSS-III is managed by the Astrophysical Research Consortium for the Participating Institutions of the
 5 SDSS-III Collaborations. The paper has made use of the LTS_LINFIT package (www-astro.physics.ox.ac.uk/~mxc/software) and
 6 the MPFIT package (<https://pages.physics.wisc.edu/~craigm/idl/cmpfit.html>).

REFERENCES

- Ahumada, R.; Prieto, C.; Almeida, A., et al., 2020, *ApJS*, 249, 3
- Baldwin, J. A.; Phillips, M. M.; Terlevich, R., 1981, *PASP*, 93, 5 - 19
- Balogh, M. L.; Morris, S. L.; Yee, H. K. C.; Carlberg, R. G.; Ellingson, E., 1999, *ApJ*, 527, 54
- Baron, D.; Netzer, H.; Prochaska, J. X.; et al., 2018, *MNRAS*, 480, 3993
- Brinchmann, J.; Charlot, S.; White, S. D. M.; Tremonti, C.; Kauffmann, G.; Heckman, T.; Brinkmann, J., 2004, *MNRAS*, 351, 1151
- Bruzual A. G.; Charlot, S., 1993, *ApJ*, 405, 538
- Cappellari, M.; Scott, N.; Alatalo, K.; et al., 2013, *MNRAS*, 432, 1709
- Cappellari, M., 2017, *MNRAS*, 466, 798
- Chadayammuri, U.; Tremmel, M.; Nagai, D.; Babul, A.; Quinn, T., 2021, *MNRAS*, 504, 3922
- Chen, Y.; Kauffmann, G.; Tremonti, C. A.; et al., 2012, *MNRAS*, 421, 314
- Cid Fernandes, R.; Mateus, A.; Sodre, L.; Stasinska, G.; Gomes, J. M., 2005, *MNRAS*, 358, 363
- Cid Fernandes, R.; Stasinska, G.; Mateus, A.; Vale Asari, N., 2011, *MNRAS*, 413, 1687
- Cid Fernandes, R.; Perez, E.; Garcia Benito, R.; et al., 2013, *A&A*, 557, 86
- Comerford, J. M.; Negus, J.; Muller-Sanchez, F., et al., 2020, *ApJ*, 901, 159
- Davies, R. I.; Burtscher, L.; Rosario, D.; Storch-Bergmann, T.; Contursi, A.; et al., 2015 *ApJ*, 806, 127
- Fabian, A. C., 2012, *ARA&A*, 50, 455
- Feruglio, C.; Maiolino, R.; Piconcelli, E., et al., 2010, *A&A*, 518, 155
- Gaspari, M.; Brighenti, F.; Temi, P., 2012, *MNRAS*, 424, 190
- Greene, J. E.; Ho, L. C., 2005, *ApJ*, 627, 721
- Heckman, T. M.; Best, P. N., 2014, *ARA&A*, 52, 589
- Kawamuro, T.; Ricci, C.; Izumi, T.; Imanishi, M.; Baba, S.; Nguyen, D. D.; Onishi, K., 2021, *ApJS*, 257, 64
- Kewley, L. J.; Groves, B.; Kauffmann, G.; Heckman, T., 2006, *MNRAS*, 372, 961 - 976
- Kewley, L. J.; Maier, C.; Yabe, K.; Ohta, K.; Akiyama, M.; Dopita, M. A.; Yuan, T., 2013, *ApJL*, 774, 10 - 15
- Kewley, L. J.; Nicholls, D. C.; Sutherland, R. S., 2019, *ARA&A*, 57, 511
- Kauffmann, G.; Heckman, T. M.; White, S. D. M.; et al., 2003a, *MNRAS*, 341, 33
- Kauffmann, G.; Heckman, T. M.; White, S. D. M.; Charlot, S.; Tremonti, C.; et al., 2003b, *MNRAS*, 341, 54
- Kauffmann, G.; Heckman, T. M.; Tremonti, C., et al., 2003, *MNRAS*, 346, 1055
- Kennicutt, J. R. C.; Tamblyn, P.; Congdon, C. E., 1994, *ApJ*, 435, 22
- Kennicutt, R. C.; Evans, N. J., 2012, *ARA&A*, 50, 501
- King, A.; Pounds, K., 2015, *ARA&A*, 53, 115
- Kolokythas, K.; O'Sullivan, E.; Giacintucci, S.; et al., 2020, *MNRAS*, 496, 1471
- Kormendy, J.; Ho, L. C., 2013, *ARA&A*, 51, 511
- Lopez Fernandez, R.; Cid Fernandes, R.; Gonzalez Delgado, R. M.; et al., 2016, *MNRAS*, 458, 184
- Ly, C.; Lee, J. C.; Dale, D. A.; Momcheva, I.; Salim, S.; Staudaher, S.; Moore, C. A.; Finn, R., 2011, *ApJ*, 726, 109
- Mahoro, A.; Povic, M.; Vaisanen, P.; Nkundabakura, P.; van der Heyden, K., 2022, *MNRAS*, 513, 4497
- Madau, P.; Dickinson, M., 2014, *ARA&A*, 52, 415
- Mahdi R.; Mohammad A., 2017, *J. Statistical Computation and Simulation*, 87, 1130
- Maraston, C.; Stromback, G., 2011, *MNRAS*, 418, 2785
- Markwardt, C. B., 2009, *Astronomical Data Analysis Software and Systems XVIII*, 411, 251
- Martinez-Paredes, M.; Aretxaga, I.; Alonso-Herrero, A.; Gonzalez-Martin, O.; Lopez-Rodriguez, E.; et al., 2017, *MNRAS*, 468, 2 - 46
- McNamara, B. R.; Nulsen, P. E. J., 2007, *ARA&A*, 45, 117
- Muller-Sanchez, F.; Nevin, R.; Comerford, J. M.; et al., 2018, *Nature*, 556, 315
- Netzer, H., 2015, *ARA&A*, 53, 365
- Netzer, H.; Lani, C.; Nordon, R.; Trakhtenbrot, B.; Lira, P.; Shemmer, O., 2016, *ApJ*, 819, 123 - 145
- Page, M. J.; Symeonidis, M.; Vieira, J. D.; et al., 2012, *Nature*, 485, 213
- Piotrowska, J. M.; Bluck, A. F. L.; Maiolino, R.; Peng, Y., 2022, *MNRAS*, 512, 1052

- Pflamm-Altenburg, J.; Weidner, C.; Kroupa, P., 2007, *ApJ*, 671, 1550
- Prieto, M. A.; Nadołny, J.; Fernandez-Ontiveros, J. A.; Mezcuca, M., 2021, *MNRAS*, 506, 562 - 580
- Richard-Laferriere, A.; Hlavacek-Larrondo, J.; Nemmen, R. S.; et al., 2020, *MNRAS*, 499, 2934
- Russell, H. R.; McNamara, B. R.; Fabian, A. C.; et al., 2019, *MNRAS*, 490, 3025
- Shin, J.; Woo, J. H.; Chung, A.; et al., 2019, *ApJ*, 881, 147
- Sanchez, S. F., 2020, *ARA&A*, 58, 12120
- Shimasaku, K.; Fukugita, M.; Doi, M.; et al., 2001, *ApJ*, 122, 1238
- Strateva, I.; Ivezić, Z.; Knapp, G. R.; et al., 2001, *AJ*, 122, 1861
- Shen, Y.; Richards, G. T.; Strauss, M. A.; et al., 2011, *ApJS*, 194, 45
- Smethurst, R. J.; Simmons, B. D.; Coil, A.; et al., 2021, *MNRAS*, 507, 3985
- Smit, R.; Bouwens, R. J.; Labbe, I.; et al., 2016, *ApJ*, 833, 254
- Suh, H.; Civano, F.; Hasinger, G.; et al., 2019, *ApJ*, 872, 168
- Tombesi, F.; Melendez, M.; Veilleux, S.; Reeves, J. N.; et al., 2015, *Nature*, 519, 436
- Tremonti, C. A.; Heckman, T. M.; Kauffmann, G.; et al., 2004, *ApJ*, 613, 898
- Villa-Velez, J. A.; Buat, V.; Theule, P.; Boquien, M.; Burgarella, D., 2021, *A&A*, 654, 153
- Werle, A.; Cid Fernandes, R.; Vale Asari, N.; Bruzual, G.; Charlot, S.; Gonzalez Delgado, R.; Herpich, F. R., 2019, *MNRAS*, 483, 2382
- Worthey, G.; Ottaviani, D. L., 1997, *ApJS*, 111, 377
- Wylezalek, D.; Zakamska, N. L., 2016, *MNRAS*, 461, 3724
- Zhang, XueGuang; Bao, M., Yuan, Q. R., 2019, *MNRAS Letter*, 490, 81
- Zhang, XueGuang; Feng, Y. Q.; Chen, H.; Yuan, Q. R., 2020, *ApJ*, 905, 97
- Zhang, XueGuang, 2021, *ApJ*, 909, 16
- Zhang, XueGuang, 2022a, *MNRAS*, 509, 4626, arXiv: 2111.07688
- Zhang, XueGuang, 2022b, *ApJS*, 261, 23, arXiv:2205.00194
- Zhang, XueGuang, 2022c, *ApJS*, 260, 31, arXiv:2203.12810
- Zhang, XueGuang, 2023, *MNRAS*, 519, 4461, arXiv: 2301.01957
- Zhuang, M.; Ho, L. C.; Shangguan, J., 2018, *ApJ*, 862, 118
- Zinn, P. C.; Middelberg, E.; Norris, R. P., et al., 2013, *ApJ*, 774, 66
- Zubovas K.; Nayakshin S.; King A.; et al., 2013, *MNRAS*, 433, 3079